Vision, Modeling, and Visualization (2013)
Michael Bronstein, Jean Favre, and Kai Hormann (Eds.)

Adaptive Surface Visualization of Vessels with Embedded Blood Flow Based on the Suggestive Contour Measure

K. Lawonn, R. Gasteiger, and B. Preim

Department of Simulation and Graphics, University of Magdeburg, Germany

Abstract

The investigation of hemodynamic information for the assessment of cardiovascular diseases (CVD) has increased in recent years. Improved flow measuring modalities and computational fluid dynamics (CFD) simulations are suitable to provide domain experts with reliable blood flow information. For a visual exploration of the flow information domain experts are used to investigate the flow information combined with its enclosed vessel anatomy. Since the flow is spatially embedded in the surrounding vessel surface, occlusion problems have to be resolved that include a meaningful visual reduction of the vessel surface but still provide important anatomical features. We accomplish this by applying an adaptive surface visualization inspired by the suggestive contour measure. Our approach combines several visualization techniques to improve the perception of surface shape and depth. Thereby, we ensure appropriate visibility of the embedded flow information, which can be depicted with established or advanced flow visualization techniques. We apply our approach to cerebral aneurysms and aortas with simulated and measured blood flow. In an informal user feedback with nine domain experts, we confirm the advantages of our approach compared with existent methods, e.g., semi-transparent surface rendering.

Categories and Subject Descriptors (according to ACM CCS): I.3.3 [Computer Graphics]: Picture/Image Generation—Line and curve generation

1. Introduction

The initiation and evolution of CVDs, such as cerebral and abdominal aneurysms, are multifactorial problems involving hemodynamics, wall biomechanics, genetics, vessel morphology, and other not well understood factors [AML*08]. In recent studies, domain experts identified certain hemodynamic information as important indicators for the presence, initiation, and outcome of a CVD [CMWP11, MFK*12]. As domain experts we consider biomedical researchers, CFD engineers, and clinicians who are involved in blood flow assessment, e.g., neuroradiologists or cardiologists. The hemodynamic information comprise quantitative measures (e.g., wall shear stress (WSS), pressure, speed) and qualitative characteristics (e.g., inflow jet, degree of vorticity), which describe the blood flow behavior. They are derived from patient-specific flow measuring with time-resolved phase-contrast MRI (4D PC-MRI) [MFK*12] or CFD simulations [CCA*05,KBDL09]. Furthermore, for particular CVDs, such as cerebral aneurysms, CFD simulations are capable to provide clinically relevant information regarding treatment options by conducting virtual treatments [AML*08]. The acquired hemodynamic information are very complex because they consist of several multivariate (e.g., scalar and vector data) and multidimensional (3D and 4D) information. In addition to a quantitative analysis an effective visual exploration of these attributes is important to obtain insights of these information. For the visual exploration domain experts are used to visualize both the flow information and the surrounding vessel anatomy because both information are strongly correlated to each other [BSH*10]. This leads to an embedded surface problem where occlusions due to the vessel surface have to be resolved in such way that important anatomical surface features are still depicted, whilst simultaneously appropriate visibility of the embedded flow visualization is ensured.

Existing techniques, such as semitransparent rendering or clipping of the vessel surface, exhibit a reduced surface shape depiction and ambiguities of the spatial relationship between vessel sections. This decreases the observers' ability to mentally link the vessel morphology with the internal

DOI: 10.2312/PE.VMV.VMV13.113-120

flow visualization. As a remedy to the problems of a semi-transparent visualization, Gasteiger et al. [GNKP10] proposed an adaptive surface visualization that incorporates a ghosted view approach. The ghosted view, leads to a completely occluded flow visualization below surface regions, which are facing away from the viewer. Furthermore, the view-dependent opacity does not ensure an appropriate depiction of salient concave and convex surface regions, which are necessary to identify pathological bulge formations of the vessel wall.

Inspired by illustrative line rendering techniques, we propose an adaptive surface rendering that overcomes these limitations. In a recent comparison of feature line approaches conducted, the *suggestive contours* technique exhibits the most effective shape description for patient-specific anatomical surfaces [LGP13]. Therefore, we developed a surface shading that incorporates the view-dependent curvature of suggestive contours into the ghosted view approach of Gasteiger et al. [GNKP10] to ensure both visibility of the embedded flow visualization and expressive depiction of salient vessel surface features.

In summary, the contributions of this paper are:

- We present a novel technique for vessel visualization with embedded blood flow information depicted with established flow visualization methods.
- We derive our method from an established feature line technique - *suggestive contours*.
- We demonstrate that our method is applicable to arbitrary vessel surfaces but also to other patient-specific anatomy.

2. Medical Background and Requirement Analysis

Cardiovascular diseases (CVD) refer to the class of diseases that effects the heart and blood flow vessels (arteries and venes). Common examples of CVDs are aortic aneurysms and dissections, cerebral aneurysms, or atherosclerosis. For the identification, progression, and risk assessment of certain CVDs the blood flow behavior plays an important role. A particular example are cerebral aneurysms, which are pathological dilations of the vessel wall that exhibit an increased risk of rupture [Juv11]. Risk factors and other relevant flow characteristics are identified by quantitative and qualitative analyses. We focus on the qualitative analysis, which involves a visual exploration of the morphology *and* its embedded blood flow information. Domain experts require the visualization of both information because they influence each other. For example, a bleb formation at the aneurysm sac indicates a previous rupture and increases the rupture risk. Blebs are high local bulges on the aneurysm sac and were found at regions of high WSS and near the flow impaction zone. Thus, an expressive surface depiction that conveys such morphological features but ensures visibility of the underlying flow is necessary.

2.1. Requirement Analysis

A detailed visual description of the enclosing vessel surface leads to an increased occlusion of internal information. Thus, an adapted surface visualization is needed to reduce the occlusion. Based on literature and discussions with domain experts, we address the following requirements:

Visibility of internal flow information: A maximum visibility of the internal flow visualization is required during the visual exploration. With "maximum visibility", we mean as few as possible occlusion of the flow visualization. This supports the viewer in interpreting and tracing the flow.

Conveying of the surface features: As vessel morphology and flow influence each other, an expressive vessel shape depiction is necessary that conveys surface features such as concave and convex regions as well as bleb formations. In contrast to Gasteiger et al. [GNKP10] no occlusion should occur for surface parts that are facing away from the viewer.

Increasing of depth perception: For the depiction of overlapping and distant vessel parts depth cues should be provided. These hints increase the perception of depth and spatial relationships of the vessel surface and attract the attention to vessel regions, which are close to the viewer.

3. Related Work

Effective embedded surface visualizations are relevant in several domains like engineering, vector field analysis, medical research, and treatment planning. Each scenario is faced with occlusions and challenges regarding perception of shape, depth, and spatial relationship. Thus, several visualization domains are involved to cope with these challenges.

Illustrative Shape Visualization. Illustrative shape visualizations aim at reproducing artistic drawings to convey surface shape details by means of shading, texturing, and pen-and-ink techniques [SABS94]. Existing approaches are mainly based on local geometry and illumination information such as normals, curvature measures, and changes of luminances. Examples of non-photorealistic shading models, which focus on surface shape enhancement, are proposed by Gooch et al. [GGSC98] and Rusinkiewicz et al. [RBD06]. Fundamental works concerning shape perception based on texture patterns were investigated by Kim et al. [KHSI04]. While all of these shading- and texture-based approaches certainly enhance surface shape, they rely on an opaque surface rendering, which is not applicable for enclosing vessel surface rendering. However, we incorporate information about the local normal orientation to convey local surface orientation such as concave and convex regions. A reduced 3D surface description can also be accomplished by illustrative line renderings such as silhouettes [IFH*03] and other features lines. Interrante et al. [IFP95] proposed ridge and valley lines, which are defined as the loci of points at which the principle curvature reaches an extremum in the principle direction. DeCarlo et al. [DFRS03] developed suggestive

contours that are defined as the set of minima of the diffuse headlight in view direction. Apparent ridges were introduced by Judd et al. [JDA07] who extend the ridge and valley lines by using view-dependent curvature and curvature direction. Xie et al. [XHT*07] presented photic extremum lines (PELs) defined as the loci of points where the variation of illumination in its gradient direction reaches a local maximum. In an informal evaluation Lawonn et al. [LGP13] figured out that suggestive contours provide the most visual pleasing results on patient-specific anatomic datasets. Depending on the flow visualization technique the generated lines and stripes on the surface may cause visual clutter in a combined visualization, e.g., in case of integral lines as flow visualization technique. Thus, we only consider silhouettes as suitable for our application.

Visualization of Embedded Structures. Fundamental research in conveying both enclosing surface shape and embedded structures was accomplished by Interrante et al. [IFP97] who investigated how sparsely-distributed opaque texturing can be used to depict the shape of transparent isointensity surfaces of radiation dose. An interactive view-dependent transparency model was proposed by Diepstraten et al. [DWE03] to improve the shape perception of embedded structures. Based on several *design rules* the transparency and visibility of the layered objects are adjusted according to the camera view and spatial relationship between opaque and semi-transparent objects. This kind of visualization is an example of ghosted views and belongs to the group of *smart visibility techniques*. These techniques focus on exposing the most important visual information and originate from technical illustration. Other examples are cut-away views, section views, and exploded views [Vio05]. A multipass framework for illustrative rendering of complex and self-occluded integral surfaces is proposed by Hummel et al. [HGH*10] and Born et al. [BWF*10]. They incorporate several rendering techniques, such as transparency modulations, hatching textures, halftoning, and illustrative streamlines, to reveal subjacent layers and to enhance shape and depth perception of each layer. In Gasteiger et al. [GNKP10], a multipass framework is presented that incorporates some of the design rules of Diepstraten et al. [DWE03] to achieve a ghosted view for enclosing vessel surfaces with embedded flow information. The opacity of the vessel surface is controlled by a Fresnel opacity term. Baer et al. [BGCP11] confirmed the performance of the visualization in a quantitative user study. However, a limitation of the ghosted view method becomes obvious in regions that are oriented away from the viewer and occlude the underlying flow visualization. Additionally, salient surface regions described by concave and convex regions may not be well conveyed by the Fresnel opacity.

Conveying Depth and Spatial Relationship. Our application is also related to conveying information of depth and spatial relationship. Two important cues for depth and spatial arrangement are shadowing and shading [WFG92]. In Luft et al. [LCD06] an image-based method is presented to integrate depth cues efficiently into complex scenes based on the differences between the depth buffer and its low-pass filtered copy. Further depth cues are atmospheric attenuation, depth blurring, and line fading, which are discussed in Svakhine et al. [SEA09]. The shadow approximation proposed by Luft et al. [LCD06] and atmospheric attenuation are also utilized by Gasteiger et al. [GNKP10] to enhance the depth perception and spatial relationship of vessel regions. Shadow-like depth indicators by means of an adaptive hatching method are proposed by Ritter et al. [RHD*06] to enable reliable comparisons of spatial distances in complex vascular structures. A weighted combination of illustrative rendering techniques is utilized by Tietjen et al. [TPB*08] for depth- and shape-enhanced medical surface visualizations inspired by medical textbook illustrations. The weighting is controlled by a *shading map*, which combines several illumination and surface information such as plateau and raking light, atmospheric attenuation, and curvature.

4. Data Acquisition Pipeline

Before we present the details of our method, we briefly describe the steps to generate the needed vascular surface and blood flow data. The data acquisition pipeline consists of three steps, illustrated in Figure 1.

Acquisition: In the first step, clinical image data (CTA, MRA, 3D rotational angiography) of the vessel are acquired. If 4D PC-MRI (phase-contrast MRI) is available, a full 3D flow measuring over time can be performed, which encodes the flow direction and magnitude at each voxel [MFK*12]. Measuring errors introduced by eddy currents, noise and velocity phase wraps are reduced according to several filter methods described in Hennemuth et al. [HFS*11].

Surface Reconstruction: In the second step, the vessel surface is reconstructed based on a vessel segmentation. Because of the high vessel-to-tissue contrast in the image data, often a simple thresholding segmentation followed by a connected component analysis is sufficient to separate the vessel from the surrounding tissue. More advanced techniques like active shape models and deformable models can be employed to minimize manual effort in cases of low intensity

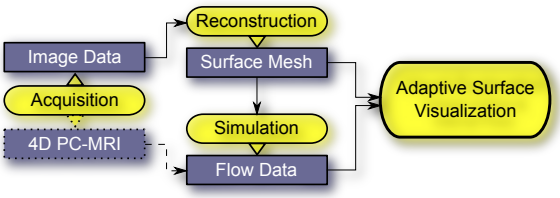

Figure 1: *Data acquisition pipeline to obtain the vessel surface and blood flow information for our approach.*

distribution [LABFL09]. The resulting segmentation mask is used to reconstruct the surface with marching cubes and optimized with respect to mesh quality by a combination of edge collapses and edge flips [Sch97].

Simulation: The optimized surface mesh is utilized for generating an unstructured volume mesh, as an input for the subsequent CFD simulation. In most cases, the blood is modeled as Newtonian fluid with steady or unsteady flow and rigid walls. Cebral et al. have shown that with these assumptions a qualitative flow characterization is still possible [CCA*05].

5. Method

Our method is based on the multipass framework proposed by Gasteiger et al. [GNKP10] and incorporates different visualization techniques, as illustrated in Figure 2. We improve the ghosted view approach by modifying the vessel opacity of the front faces by means of the suggestive contour measure. Furthermore, we utilize depth blurring instead of atmospheric attenuation because of the more natural depth perception. We first recap the suggestive contours technique and present its incorporation into our modified ghosted view shading approach afterwards.

5.1. Suggestive Contours

Suggestive contours are view-dependent feature lines based on second order derivatives. These lines are defined as the set of minima of $n \cdot v$ in the direction of w, where n is the unit surface normal, v is the view vector (which points to the camera), and w is the projection of the view vector on the tangent plane. Precisely:

$$D_w(n \cdot v) = 0, \text{ and } D_w D_w(n \cdot v) > 0.$$

First, one has to evaluate $n \cdot v$ per vertex. Afterwards, the gradient $\nabla(n \cdot v)$ is determined for each triangle $t = (p_1, p_2, p_3)$. Every vertex p_1, p_2, p_3 obtains a scalar value. These values are calculated by the dot product of the associated vertex normal n_j, $j \in \{1,2,3\}$ and the view vector v:

$$l = \begin{pmatrix} \langle n_1, v \rangle & \langle n_2, v \rangle & \langle n_3, v \rangle \end{pmatrix}^T. \tag{1}$$

Every triangle requires an (u,v) orthonormal coordinate system. We write the u and v component in one vector, respectively:

$$U = \begin{pmatrix} \langle p_1, u \rangle & \langle p_2, u \rangle & \langle p_3, u \rangle \end{pmatrix}^T \tag{2}$$

and

$$V = \begin{pmatrix} \langle p_1, v \rangle & \langle p_2, v \rangle & \langle p_3, v \rangle \end{pmatrix}^T. \tag{3}$$

The light gradient ∇l of the triangle is determined by:

$$\nabla l = \frac{1}{A} \begin{pmatrix} (V \times \mathbb{1})^T \\ -(U \times \mathbb{1})^T \end{pmatrix} l^i, \tag{4}$$

where A denotes the area of the current triangle and $\mathbb{1} = (1\ 1\ 1)^T$. Next, we use the triangle gradient to determine the vertex gradient. For this purpose, we consider the adjacent triangles of a vertex and rotate each face gradient into the vertex's tangent space. Afterwards, we average the gradients according to their voronoi area, as described by Meyer et al. [MDSB02], and obtain the light gradient $l_i = \nabla(n_i \cdot v)$ for the i-th vertex. Finally, given the view vector v, the light gradient l_i, and the corresponding normalized vertex normal n_i, we project v onto the tangent space of the i-th vertex. So we get $w_i = v - n_i^T n_i \cdot v$. The feature lines are defined as the zero-crossing of the dot product $w_i \cdot l_i$ by linearization in the interior of a triangle. Furthermore, lines are drawn if the derivative magnitude is larger than a user-defined threshold. However, objects without concave regions have no *suggestive contours*.

5.2. Feature Regions

Our shading is defined by the value of $s_i = w_i \cdot l_i$ with the values defined in Subsection 5.1. Prominent highlights are defined as zero-crossings of s_i and we convey these regions with an expressive color coding. Thereby, we differentiate between negative and positive values of s_i. To differentiate the regions, we choose two antipodal colors in the CIELab colorspace. First, we choose a color $col_1 = \{L,a,b\}$, in our case orange with $col_1 = \{65,51,74\}$, and change the signs of a,b. So, we get $col_2 = \{L,-a,-b\}$, in our case $col_2 = \{65,-51,-74\}$. Therefore, we obtain two different colored regions where the border represents a feature derived by *suggestive contours*. Additionally, we multiply the value $c \cdot |s_i|$ with the corresponding color and add them to the backface color of the vessel. Here, c is a user-defined value, which adjusts the brightness of the shading. That means, whenever we have a low value of s_i, we get a color which is nearly black. The result is a shading, which conveys the impression of a Fresnel opacity with highlighted surface features.

5.3. Visual Effects

We added some visual effects to emphasize the region of interest. First, we apply an approximated shadow casting onto the front faces of the vessel surface to enhance spatial relationship between overlapping vessel sections. Here, we implemented the method proposed by Luft et al. [LCD06] and compute a *spatial importance function* from the depth buffer and its low-pass filtered version. The low-pass filtering is accomplished by a Gaussian blurring and the result is substracted from the original depth buffer. Negative values represent areas of background objects that are close to other occluding objects. The shadow casting is approximated by adding the negative values to the original color values, which causes a local darkening.

Furthermore, we consider a focus region as a basis for focus-and-context visualization as well as depth attenuation. This region is defined by a depth-near and depth-far region adjusted by the user and may represent pathological regions

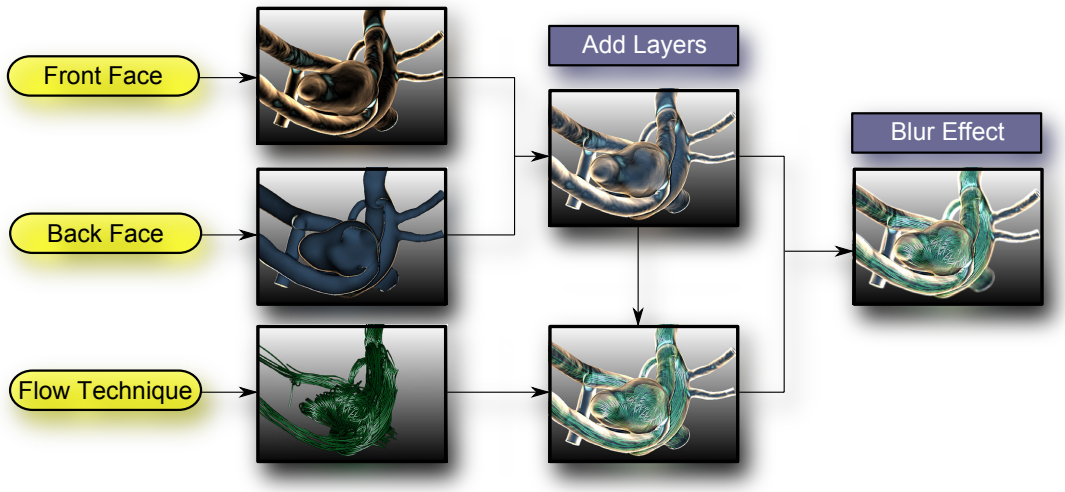

Figure 2: *Overview of our adaptive surface visualization: First, we render the vessel front faces and encode the transparency according to the suggestive contour measure. The back faces are rendered opaque and the flow is visualized with established flow visualization techniques, e.g., streamlines. Second, we compose each visualization layer and add shadow approximation as well as depth blurring to the result.*

such as the aneurysm sac or stenosis. Vessel sections, which are outside this region, will be blurred according to a Gaussian blurring filter with a kernel size that depends linearly on the distance between vessel sections and the focus region. This leads to a smooth transition between the focus region and the surrounding that supports both attraction to the focus region and perception of depth. The blurred vessel sections with their embedded flow visualization are still provided as context information (see Fig. 2, right).

6. Algorithm and GPU Implementation

The algorithm of our shading is as follows:

1. (Optional) Subdivide and smooth the mesh.
2. Compute vertex normals.
3. Build neighbor information.
4. Determine vertex gradient.
5. Compute color for each vertex.
6. Blur the rendered image and add shadows.

The algorithm is divided in two different parts. The first part (1-3) consists of the preprocessing steps and the second part (4-6) is executed during runtime. For achieving a fast rendering, several APIs, such as CUDA, OpenCL, or DirectCompute are available. To be independent of graphics card vendors and to reduce any overhead by additional APIs, we chose to perform all computations with the OpenGL shader framework. The shader concept is ideally suited for per-vertex and per-triangle operations. OpenGL shaders do natively not provide neighborhood information, such as the 1-ring of each vertex. Therefore, we develop a data structure to access the neighbor of a vertex.

6.1. Preprocessing

First, we compute the vertex normals by averaging the area-weighted normals over adjacent faces. For the neighborhood information of a vertex, we use the OpenGL extension GL_ARB_SHADER_STORAGE_BUFFER_OBJECT, which is part of the OpenGL core since version 4.3. With this, we create a 4-dimensional integer vector. The first component consists of the ordered neighbors of the vertices. The second component stores the number of neighbors in the associated list entry. In the third component, we write the offset index where we can find the entry for the first component. The last component consist of zeros.

6.2. Rendering Loop

During runtime, steps 4, 5, and 6 are executed. Using vertex shaders, we can determine the vertex gradient, which depends on the camera position and the light position. We use the fragment shader to assign the color per pixel and to perform the Gaussian blur on the one hand, and to determine the shadows on the other hand. Therefore, we divide the calculation in two shaders. The first one assigns the color and the second one performs the blurring and the shadow effects, described in Section 5.3.

7. Evaluation

We performed an informal evaluation for the three shading techniques: semitransparency ($\mathbf{ST}_1$), fresnel opacity $\mathbf{ST}_2$ according to Gasteiger et al. [GNKP10], and our shading $\mathbf{ST}_3$ based on the suggestive contour measure, see Figure 3.

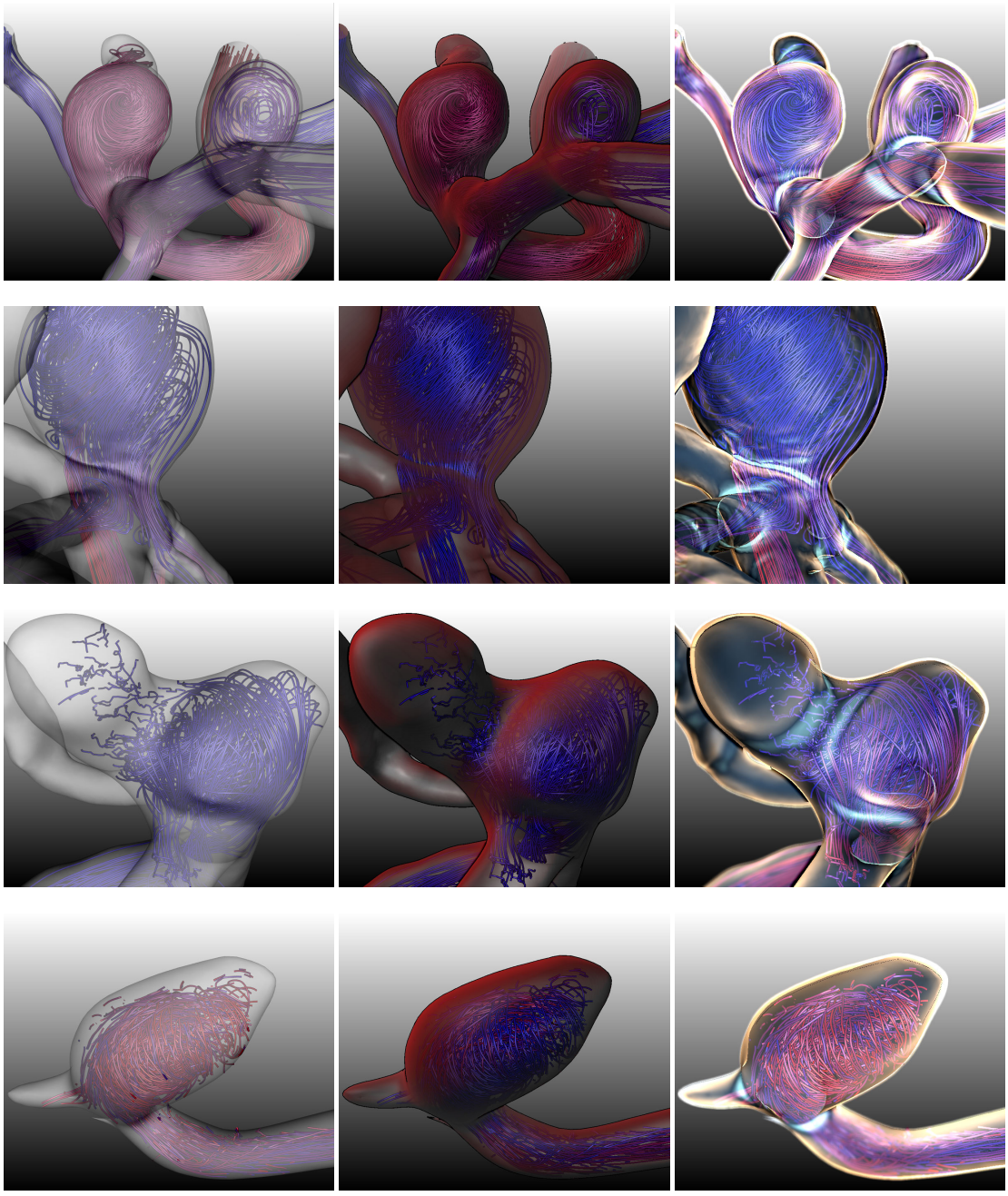

Semitransparency | Fresnel opacity [GNKP10] | Our shading

Figure 3: *Our shading in comparison with semitransparent visualization and Fresnel opacity [GNKP10] for different vessels with internal flow depicted with illustrative streamlines. The semitransparent approach fails to give a spatial impression. The Fresnel opacity approach provides good visual results but some streamlines are occluded by fully opaque vessel regions facing away from the viewer. Our approach overcomes these limitations and the streamlines are depicted well.*

The goal was to assess their capabilities for expressing relevant surface characteristics whilst simultaneously gaining appropriate visibility of the embedded streamline visualization. We wanted to figure out which of the proposed shading techniques yields the most expressive results. Therefore, we conducted an evaluation with one physician, two CFD engineers involved in hemodynamic analysis, and six researchers with background in medical visualization. We chose four representative vessel structures consisting of three cerebral aneurysms and one aorta dataset. During the evaluation, we noted the participants' spoken comments and the participants were able to adjust the parameter settings for each technique, i.e., transparency value for $\mathbf{ST}_1$, edge fall-off parameter for $\mathbf{ST}_2$, and brightness value c for $\mathbf{ST}_3$ (recall Sec. 5.2). For each dataset and technique the participants were asked to perform three tasks:

1. Identification of salient surface features such as concave, convex regions and performance assessment of each shading technique to accomplish the task.
2. Visibility assessment of the embedded streamlines.
3. Assessment of spatial relationship and depth perception between vessel sections.

For *task 1*, technique $\mathbf{ST}_3$ was rated as most effective and revealed more surface features compared to $\mathbf{ST}_1$ and $\mathbf{ST}_2$. The participants stated that certain curvature features at branches and bulges on the aneurysm sac were more clearly depicted in $\mathbf{ST}_3$ than in $\mathbf{ST}_1$ and $\mathbf{ST}_2$ (see Fig. 3, third row). An increase of the opacity for $\mathbf{ST}_1$ improved the perception but also increased the occlusion to the embedded streamlines. Therefore, technique $\mathbf{ST}_2$ was rated better than $\mathbf{ST}_1$ because an increased edge fall-off reveals more shape features but still ensures visibility of the flow facing towards the viewer. Most of the participants also appreciated the capability of $\mathbf{ST}_3$ to convey the salient surface features even in still images. For some vessel structures the other two techniques required more camera interaction efforts to obtain an overview about the shape.

The assessment in *task 2* was rated most effective for technique $\mathbf{ST}_3$ when using a brightness value around 1.5. Larger values would occlude more streamlines, which is similar to $\mathbf{ST}_2$ in terms of the edge fall-off value (in average 1.5). For this technique, some participants criticized the increased occlusion of surface parts facing away from the viewer. As expected for $\mathbf{ST}_1$ an increased transparency improves also the streamline visibility but decreases the shape depiction. Some participants stated that this assessment depends on the exploration task, i.e, focusing on embedded flow or on flow and enclosing vessel.

For *task 3*, $\mathbf{ST}_2$ and $\mathbf{ST}_3$ were rated as most effective compared to $\mathbf{ST}_1$ because of the added shadow and depth cues. Thereby, blurring and depth attenuation were evaluated equally expressive with slightly more preference for blurring because of its more natural adaption to the human depth perception. Two participants also asked for a possibility to change the region of interest for the focus region by clicking on a specific vessel region.

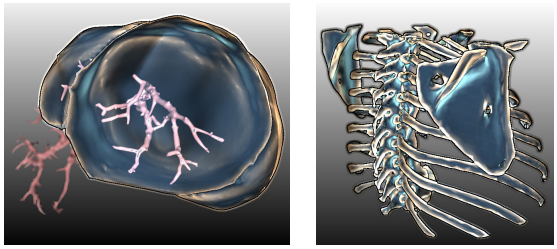

Figure 4: *Our adaptive surface approach can also be applied to non-vessel surfaces such as (a) liver surfaces with portal vein and (b) bone structures.*

8. Conclusion and Future Work

In this paper, we have presented a novel adaptive surface visualization technique for blood vessels with embedded flow information. The shading technique is based on the *suggestive contour* measure, which ensures both an appropriate depiction of relevant local surface features and visibility of the embedded flow visualization. Furthermore, we incorporate depth blurring to an enhanced depth and spatial relationship. Our informal evaluation with domain experts demonstrated an improved shape perception compared to existing techniques whilst simultaneously ensure appropriate visibility of the embedded flow visualization. Moreover, our approach is capable to convey the salient surface features in still images, which also enables its utilization for documentation purposes. Besides its application on vessels with embedded flow information our approach is also applicable to other non-vessel surfaces such as liver surfaces with internal structures and bone structures, as shown in Figure 4.

For future work, we consider a controlled user study to quantify the performance of our approach compared to a semitransparent vessel visualization and the ghosted view approach by Gasteiger et al. [GNKP10]. This study is oriented to the work of Baer et al. [BGCP11] and includes task-driven experiments such as adjusting of surface normals or distance estimations of vessel sections. The quantitative performance of each shading technique can be assessed based on the accuracy and response time of each task.

Acknowledgments

The authors wish to thank P. Berg, U. Preim, and D. Stucht for their feedback.

References

[AML*08] Appanaboyina S., Mut F., Löhner R., Putman C., Cebral J.: Computational Fluid Dynamics of Stented Intracranial Aneurysms Using Adaptive Embedded Unstructured Grids. *Numerical Methods in Fluids 57*, 5 (2008), 475–493. 1

[BGCP11] Baer A., Gasteiger R., Cunningham D. W., Preim B.: Perceptual evaluation of ghosted view techniques for the exploration of vascular structures and embedded flow. *Computer Graphics Forum 30*, 3 (2011), 811–820. 3, 7

[BSH*10] Baharoglu M. I., Schirmer C. M., Hoit D. A., Gao B.-L., Malek A. M.: Aneurysm Inflow-Angle as a Discriminant for Rupture in Sidewall Cerebral Aneurysms Morphometric and Computational Fluid Dynamic Analysis. *Stroke 41*, 7 (2010), 1423–1430. 1

[BWF*10] Born S., Wiebel A., Friedrich J., Scheuermann G., Bartz D.: Illustrative Stream Surfaces. *IEEE Transactions on Visualization and Computer Graphics 16*, 6 (2010), 1329–1338. 3

[CCA*05] Cebral J. R., Castro M. A., Appanaboyina S., Putman C. M., Millan D., Frangi A. F.: Efficient Pipeline for Image-Based Patient-Specific Analysis of Cerebral Aneurysm Hemodynamics: Technique and Sensitivity. *IEEE Trans. Med. Imaging 24*, 4 (2005), 457–467. 1, 4

[CMWP11] Cebral J. R., Mut F., Weir J., Putman C. M.: Association of Hemodynamic Characteristics and Cerebral Aneurysm Rupture. *American Journal of Neuroradiology 32*, 2 (2011), 264–270. 1

[DFRS03] DeCarlo D., Finkelstein A., Rusinkiewicz S., Santella A.: Suggestive contours for conveying shape. *Proc. ACM SIGGRAPH* (2003), 848–855. 3

[DWE03] Diepstraten J., Weiskopf D., Ertl T.: Interactive Cutaway Illustrations. *Computer Graphics Forum 22*, 3 (2003), 523–532. 3

[GGSC98] Gooch A., Gooch B., Shirley P., Cohen E.: A non-photorealistic lighting model for automatic technical illustration. In *Proc. ACM SIGGRAPH* (1998), pp. 447–452. 2

[GNKP10] Gasteiger R., Neugebauer M., Kubisch C., Preim B.: Adapted Surface Visualization of Cerebral Aneurysms with Embedded Blood Flow Information. In *Eurographics Workshop Vis. Comput. for Bio. and Med. (EG VCBM)* (2010), pp. 25–32. 2, 3, 4, 6, 7

[HFS*11] Hennemuth A., Friman O., Schumann C., Bock J., Drexl J., Markl M., Peitgen H.-O.: Fast Interactive Exploration of 4D MRI Flow Data. In *Proc. SPIE Medical Imaging* (2011). 3

[HGH*10] Hummel M., Garth C., Hamann B., Hagen H., Joy K. I.: Iris: Illustrative Rendering for Integral Surfaces. *IEEE TVCG 16*, 6 (2010), 1319–1328. 3

[IFH*03] Isenberg T., Freudenberg B., Halper N., Schlechtweg S., Strothotte T.: A Developer's Guide to Silhouette Algorithms for Polygonal Models. *IEEE Computer Graphics and Applications 23*, 4 (2003), 28–37. 2

[IFP95] Interrante V., Fuchs H., Pizer S.: Enhancing transparent skin surfaces with ridge and valley lines. In *Proceedings of the 6th conference on Visualization 1995* (1995), pp. 52–59. 2

[IFP97] Interrante V., Fuchs H., Pizer S. M.: Conveying the 3D Shape of Smoothly Curving Transparent Surfaces via Texture. *IEEE Trans. on Visualization and Computer Graphics (TVCG) 3*, 2 (1997), 98–117. 3

[JDA07] Judd T., Durand F., Adelson E.: Apparent ridges for line drawing. In *ACM SIGGRAPH 2007 papers* (2007), p. 19. 3

[Juv11] Juvela S.: Prevalence of and risk factors for intracranial aneurysms. *The Lancet Neurology 10*, 7 (2011), 595–597. 2

[KBDL09] Karmonik C., Bismuth J., Davies M., Lumsden A.: Computational fluid dynamics as a tool for visualizing hemodynamic flow patterns. *Methodist Debakey Cardiovasc J 5*, 3 (2009), 26–33. 1

[KHSI04] Kim S., Hagh-Shenas H., Interrante V.: Conveying shape with texture: Experimental investigations of texture's effects on shape categorization judgments. *IEEE Transactions on Visualization and Computer Graphics 10*, 4 (2004), 471–483. 2

[LABFL09] Lesage D., Angelini E. D., Bloch I., Funka-Lea G.: A Review of 3D Vessel Lumen Segmentation Techniques: Models, Features and Extraction Schemes. *Medical Image Analysis 13*, 6 (2009), 819–845. 4

[LCD06] Luft T., Colditz C., Deussen O.: Image enhancement by unsharp masking the depth buffer. In *ACM Trans. on Graphics (TOG)* (2006), vol. 25, pp. 1206–1213. 3, 4

[LGP13] Lawonn K., Gasteiger R., Preim B.: Qualitative evaluation of feature lines on anatomical surfaces. In *Bildverarbeitung für die Medizin* (2013), pp. 187–192. 2, 3

[MDSB02] Meyer M., Desbrun M., Schröder P., Barr A. H.: Discrete differential-geometry operators for triangulated 2-manifolds. In *Proc. VisMath* (2002), pp. 35–57. 4

[MFK*12] Markl M., Frydrychowicz A., Kozerke S., Hope M., Wieben O.: 4d flow mri. *Journal of Magnetic Resonance Imaging 36*, 5 (2012), 1015–1036. 1, 3

[RBD06] Rusinkiewicz S., Burns M., DeCarlo D.: Exaggerated shading for depicting shape and detail. *Proc. ACM SIGGRAPH 25*, 3 (2006). 2

[RHD*06] Ritter F., Hansen C., Dicken V., Konrad O., Preim B., Peitgen H.-O.: Real-Time Illustration of Vascular Structures. *IEEE Trans. on Visualization and Computer Graphics* (2006), 877–884. 3

[SABS94] Salisbury M. P., Anderson S. E., Barzel R., Salesin D. H.: Interactive pen-and-ink illustration. In *Proc. ACM SIGGRAPH* (1994), ACM, pp. 101–108. 2

[Sch97] Schöberl J.: NETGEN: An Advancing Front 2D/3D-Mesh Generator Based on Abstract Rules. *Computing and Visualization in Science 1* (1997), 41–52. 4

[SEA09] Svakhine N. A., Ebert D. S., Andrews W. M.: Illustration-inspired depth enhanced volumetric medical visualization. *Visualization and Computer Graphics, IEEE Transactions on 15*, 1 (2009), 77–86. 3

[TPB*08] Tietjen C., Pfisterer R., Baer A., Gasteiger R., Preim B.: Hardware-Acceelerated Illustrative Medical Surface Visualization with Extended Shading Maps. In *Proc. of SmartGraphics* (2008), pp. 166–177. 3

[Vio05] Viola I.: *Importance-Driven Expressive Visualization*. PhD thesis, Institute of Computer Graphics and Algorithms, Vienna University of Technology, June 2005. 3

[WFG92] Wanger L. R., Ferwerda J., Greenberg D. P.: Perceiving spatial relationships in computer-generated images. *IEEE Computer Graphics and Applications 12*, 3 (1992), 44–58. 3

[XHT*07] Xie X., He Y., Tian F., Seah H.-S., Gu X., Qin H.: An effective illustrative visualization framework based on photic extremum lines (pels). *IEEE Transactions on Visualization and Computer Graphics 13* (2007), 1328–1335. 3